Anal. Bioanal. Electrochem., Vol. 15, No. 11, 2023, 988-1000
https://www.doi.org/10.22034/abec.2023.709115

Analytical &
Bioanalytical
Electrochemistry

2023 by CEE
www.abechem.com

Full Paper

Influence of Current Density onto Composition and Corrosion of Electrodeposited Ni–Zn Alloys

Naima Benachour, * and Rana Amiri

Department of Chemistry, Faculty of Science, University of 20 August 1955-Skikda, Algeria

*Corresponding Author, Tel.: +213797006837
E-Mail: naimabenachour2018@gmail.com

Received: 21 May 2023 / Received in revised form: 16 October 2023 /
Accepted: 20 November 2023 / Published online: 30 November 2023

Abstract- The initial corrosion rates of electrodeposited Zn-Ni coating under galvanostatic conditions are closely related to the current density. The NH_4Cl 12-14 wt% Ni coating showed better corrosion resistance than the other investigated coatings due to the lower Ni content of 9 wt%. Moreover, nodular granules closely packed with capillary fissures, along with the formation of the electrochemically noble γ-Ni_5Zn_{21} phase, were observed at the highest Ni concentration of 10 wt%. The results of electrochemical characterization on the copper substrate showed an extended testing time, indicating a nobler corrosion potential. Additionally, the grain size refines with the presence of NH_4Cl, and the increase in cathodic current density can also lead to a decrease in grain size.

Keywords- Electroplating;grain; Microstructure; Electrodeposition; XRD

---

1. INTRODUCTION

It is known that Zn-Ni alloy coatings are used as anti-corrosion coatings, gaining significant attention due to their potential to replace cadmium coatings which are carcinogenic and toxic in nature [1,2]. Zn-Ni alloy coatings, containing up to 12% Ni, provide cathodic protection to iron (Fe), which determines their anti-corrosion performance. Numerous studies have shown that the optimal Ni content is typically found within the range of 10-15 wt% Ni with the remaining portion being Zn. This composition corresponds to the formation of a single γ phase (Ni5Zn21) [3,4]. Despite this, the corrosion behavior of Zn-Ni electrodeposits with Ni content less than 10 wt% has not been thoroughly investigated.

It is essential to analyze the corrosion behavior of Zn-Ni alloys with low Ni concentrations, ranging from 4 to 10 wt%, as they offer improved corrosion resistance compared to pure Zn. Maintaining sacrificial protection throughout corrosion can lead to enhanced formability and reduced internal stress. However, Zn-Ni alloys with nickel contents exceeding 10 wt% exhibit decreased formability due to the significantly increased hardness of the deposits. Complexing agents play a crucial role in achieving a stable Zn-Ni plating bath. Specifically, we are interested in studying the impact of ammonium chloride on Zn-Ni electroplating. However, the hydrogen evolution reaction that occurs during electrodeposition significantly affects the quality of the Zn-Ni deposit and the current efficiency. In some cases, the substrate might also be susceptible to hydrogen embrittlement as a result of this process

To evaluate the corrosion protection and sacrificial properties of these coatings, galvanic coupling tests were conducted between stainless steel samples and copper coated with Zn-Ni. The structure, grain size, and nickel content are clearly dependent on the current density and the additives used, as characterized by scanning electron microscopy (SEM) and X-ray diffraction (XRD). In this article, galvanostatic electrodepositing methods were utilized to investigate the deposition and phases of zinc-nickel coatings, exploring their responses to different electrode potentials, alloy surface composition, and the presence or absence of NH_4Cl. Electrodeposition of Zn-Ni alloy coatings containing more than 10% Ni was carried out in an acidic chloride bath. The influence of nickel content within the electrodeposits on the alloy's electrochemical characteristics was thoroughly examined, with a primary focus on the structural and morphological evolution. Potentiodynamic curves and electrochemical impedance spectroscopy (EIS) methods were employed to analyze the corrosion behavior of the electrodeposited Zn-Ni alloys in an acidic environment. Electrodepositing additives served various functions such as grain refinement, controlling Ni content, influencing chemical composition, and subsequently affecting corrosion behavior. Grain refinement and Ni content are closely related to inhibition, thereby impacting nucleation and growth processes.

In this paper, a novel acidic Zn-Ni alloy bath incorporating NH_4Cl as the complexing agent was developed to investigate the role of additives in microstructure development during electrodeposition. The impact of cathode current density and substrate on Ni content, as well as cathode current efficiency, was studied. Simultaneously, electrochemical behavior was examined through polarization curves and EIS to elucidate how Ni content influences phase structure, surface morphology, and grain size, all of which collectively contribute to the corrosion resistance of the deposits.

2. EXPERIMENTAL SECTION

The electrolyte solution used consists of H_3BO_3: 0.1 M, $ZnCl_2$: 1.8 M, and $NiCl_2.6H_2O$: 1.1 M. The substrates are stainless steel (AISI 304) plates and copper with a surface area of 1 cm^2. To ensure reproducibility in the experiments, the electrode surface is meticulously prepared before each deposition, following these steps: initial surface polishing with glasspaper from #1200 to #4000, subsequent polishing with an ESCIL felt pad using an alumina suspension with a grain size of 1 µm, and concluding with a distilled water rinse. The pH of the solution is maintained at 4.86 and 3.73, and the temperature is regulated at 30°C. For electrodeposition, an Ag/AgCl reference electrode is used, with a platinum anode acting as the counter electrode. The substrates under study (AISI 304, copper) are connected as the cathode. Ni-Zn alloy electrodeposition is carried out using a constant current mode at 30°C for a duration of 30 minutes. After electrodeposition, the samples are cleaned with distilled water.

Phase composition analysis is performed using an X-ray diffractometer (Bruker D8 Advance) with Cu monochromatic radiation (λ = 1.54 Å). Chemical composition and surface morphology are examined using scanning electron microscopy (SEM) (JEOL JSM 6460LA microscope with an EDS JEL1300 microprobe). The electrochemical cell is linked to an AUTO LAB measurement device that incorporates a potentiostat/galvanostat. This setup is connected to a microcomputer and controlled by NOVA 2.0 software. The corrosive environment is created using an HCl 0.1 M solution. The corrosion behavior analysis of electrodeposited Zn-Ni coatings is conducted through potentiodynamic polarization methods. A three-electrode system with a 0.1 M chloride acid (HCl) solution is employed. An Ag/AgCl electrode serves as the reference electrode and platinum foil functions as the counter electrode. The working electrodes consist of substrates with a 1 cm2 area, covered with Zn-Ni coatings. The bath temperature is maintained at 25°C, and the scan rate for the polarization curves is set at 1 mV/s.

3. RESULTS AND DISCUSSION

3.1. Deposition process

Figure 1 illustrates the potential-time relationship for the deposition of Zn-nickel alloys on a steel substrate at two different current levels. In the absence of NH_4Cl, the $E\tau$ (nucleation potential) shifts to a more negative potential, and the $T\tau$ (nucleation time) decreases with lower cathode current density values, indicating a faster deposition kinetics. At -20 mA/cm^2, immediate potential drop to around -2.61 V occurs upon immersion, and deposition proceeds with minimal nucleation overpotential in both cases. The curve plateau responds to an increased Zn content due to the formation of new ZnNi phases.

Under weak polarization conditions, nickel deposition is significantly hindered by the presence of zinc, despite the induction of zinc deposition by nickel presence [5,6]. Additionally, with the additive (NH_4Cl), the gradual decline in potentials corresponds to an increase in hydrogen release at the electrode surface caused by NH_4Cl discharge. It's evident that hydrogen evolution reaction is more pronounced in the presence of NH_4Cl, especially at -40 mA/cm^2, which can lead to a substantial drop in current efficiency and nucleation potential ($E\tau$), affecting the nucleation time ($T\tau$).

Increasing the cathodic current to -40 mA/cm^2 leads to more negative values of the plateau potential (around -3.58 V), required for initial nucleus formation and enhanced zinc deposition. However, in the presence of NH_4Cl, the potential shifts towards more positive values, indicating that NH_4Cl inhibits zinc deposition and promotes the formation of a Zn-Ni alloy film [7].

The results indicate that the presence of ammonium chloride in the electrolysis bath makes the drop of H^+ ions more susceptible. Consequently, certain hydrogen reactions might be triggered due to the rise in cathodic potential, leading to decreased current efficiency. At a current density of -20 mA/cm^2, the current efficiency (η) dropped by 20% compared to the result obtained without the additive. This suggests that hydrogen bubble formation might partially obstruct active sites for Ni^{2+} and Zn^{2+} reduction. With the increase in deposition cathodic current density from 20 mA/cm2 to 40 mA/cm^2, the current efficiency, calculated using the Faraday equation, increases from approximately 67% to 83%. During the electroplating process, it was observed that as the deposition current increased, hydrogen evolution became more pronounced, contributing to the decrease in current efficiency.

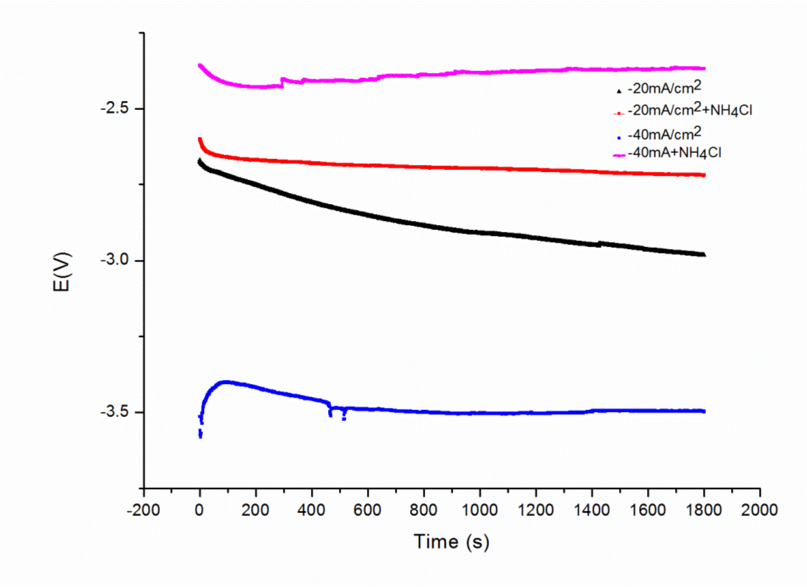

Figure 1. Zn–Ni alloy deposited under chronopotentiometry conditions (T=30 °C, t=30 min) in plating solution on stainless steel; (I= -20; -40 mA/cm^2)

3.2. *Characterization of Ni–Zn alloy*

3.2.1. The surface morphology

Figures 2 and 3 display the surface morphologies of Zn-Ni alloy coatings achieved at various current densities on two different substrates. The presence of NH_4Cl significantly impacts the morphology of the deposits, resulting in distinct differences compared to deposits obtained without NH_4Cl. Additionally; the morphology of the coatings undergoes complete transformations with varying applied current densities, as depicted in Figure 2.

The deposits appear compact, fine-grained, and fully coat the substrates. In the absence of NH_4Cl (I = -20 mA/cm^2), a uniform deposit with fine nanocrystallites of zinc-nickel (10^{-8} nm) is observed. This fine structure arises due to the increased deposition rate and the dominance of the γ-(Ni_5Zn_{22}) phase over the δ-(Ni_3Zn_{22}) phase. It's worth noting that a reduction in grain size is linked to improved passive film protection and increased corrosion resistance of deposits [8].

Dendritic grains are visible at I = -40 mA/cm^2, indicating a higher Ni content in these regions compared to the matrix, as confirmed by EDS analysis. This suggests that current density strongly influences grain size and surface morphology of Zn-Ni alloy deposits. The Ni content in deposits is also significantly affected by current density, as observed in Figure 2 (a, b).

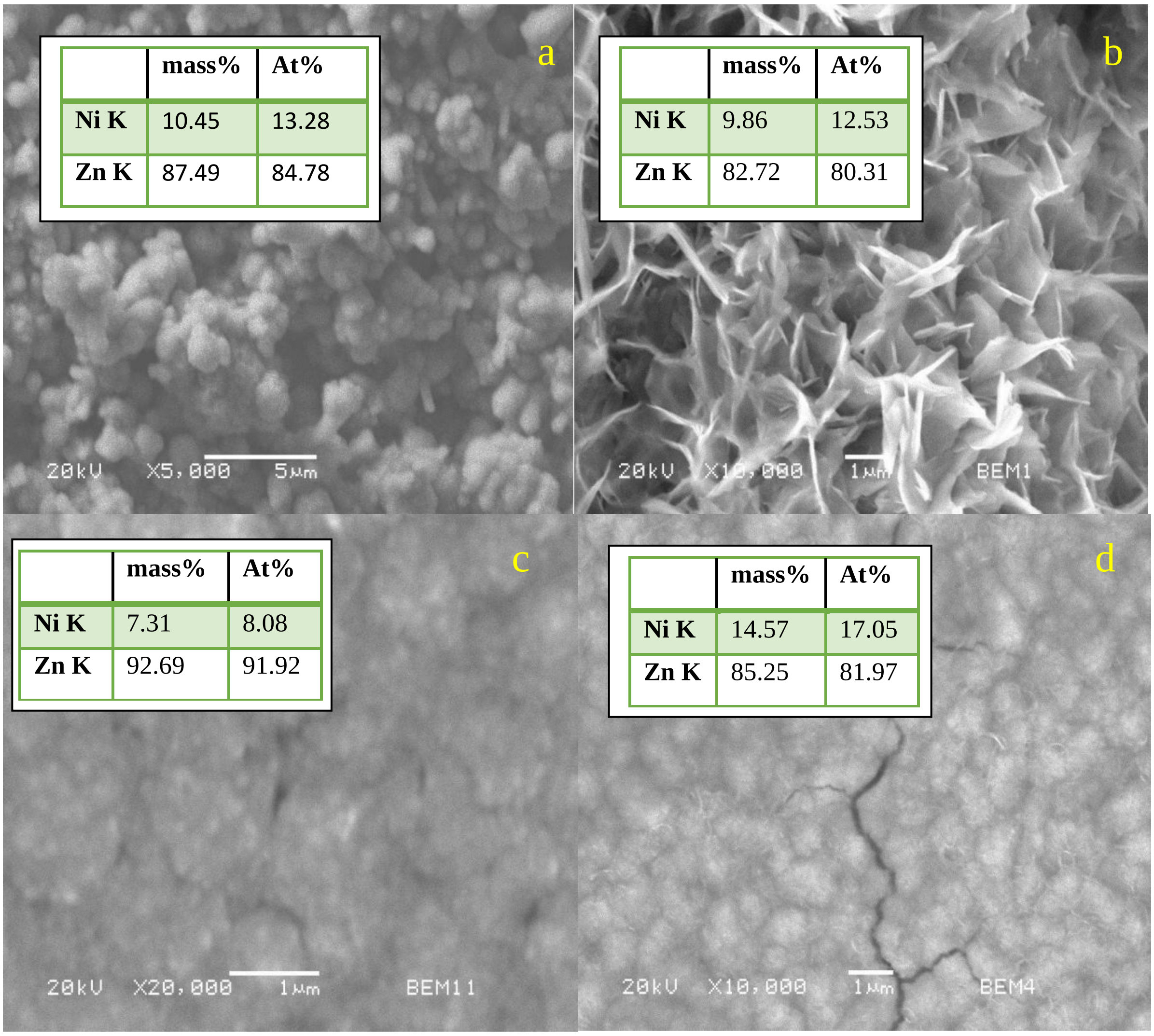

a

	mass%	At%
Ni K	10.45	13.28
Zn K	87.49	84.78

b

	mass%	At%
Ni K	9.86	12.53
Zn K	82.72	80.31

c

	mass%	At%
Ni K	7.31	8.08
Zn K	92.69	91.92

d

	mass%	At%
Ni K	14.57	17.05
Zn K	85.25	81.97

Figure 2. Optical and MEB surface morphologies Zn–Ni-coated AISI304 steel in plating bath and measurement. (a) -20 mA/cm^2 ;(b) -40 m/cm^2 ;(c) -20 mA/cm^2+NH_4Cl;(d) -40 m/cm^2

In the presence of NH_4Cl (Figure 2c) at I = -20 mA/cm^2, nodules of uniform size are apparent on the substrate's surface. These nodules are distributed across the substrate's surface, forming a granular-type deposit composed of small crystallites with sizes around 16.6 nm. XRD pattern results indicate a combination of η-phase and γ-phase in the deposits. The nanoscale nodular morphology of the coating suggests that the formation of crystal nuclei is simpler compared to their growth.

At I = -40 mA/cm^2 (Figure 2d), some cracks are observed, possibly attributed to hydrogen reduction due to the pH effect. The additive also significantly impacts the grain size of the coatings on the copper substrate (Figure 3). The size of nanocrystalline deposits is calculated using Scherrer's formula based on XRD results.

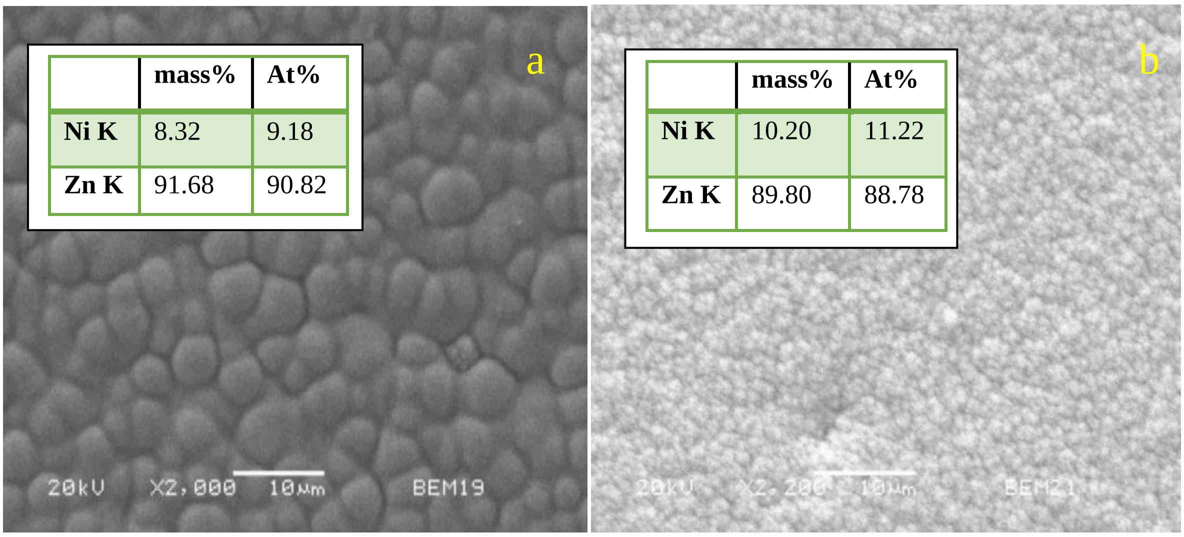

	mass%	At%
Ni K	8.32	9.18
Zn K	91.68	90.82

	mass%	At%
Ni K	10.20	11.22
Zn K	89.80	88.78

Figure 3. Optical and MEB surface morphologies Zn–Ni-coated cupper in plating and EDX measurement; (a) -20 mA/cm^2;(b) ;(c) -20 mA/cm^2+NH_4Cl

3.2.2. Phase structure of the deposit

The phase structures of the coatings obtained on the stainless-steel substrate were analyzed using X-ray diffraction (XRD), as shown in Figure 4. The XRD pattern displays two prominent peaks and additional weaker peaks corresponding to γ-Ni_5Zn_{21} and pure zinc phases, which are characteristic of Zn-Ni alloy electrodeposition. In our study, the majority of samples contain more than 10%wt Ni, with the predominantly observed phase being the γ-phase. At the same time, only the γ-phase is predominantly observed.

The deposits exhibit a η-phase structure with low Ni content (8.08 at.%) at -20 mA/cm^2 when NH_4Cl is present. By increasing the cathodic current density to -40 mA/cm^2 in the presence of NH_4Cl, a single γ-phase structure with a body-centered cubic arrangement can be achieved. EDS analysis confirms that the Ni content in these coatings is 17.05 at.%. It's noteworthy that the current density significantly influences the phase structure of the deposits in the presence of NH_4Cl.

Furthermore, coatings with Ni content ranging from 14.62 wt.% to 12.94 wt.% are characterized by a γ-phase structure. Hence, Ni content has a substantial impact on the phase structure of Zn-Ni alloys. As Ni content in deposits increases, Zn-Ni intermetallic phases with higher Ni percentages are formed. The peak intensity of the γ-phase with (411) plane orientation is more pronounced compared to other orientations, indicating that the γ-phase with (411) plane orientation predominantly influences coatings with a single γ-phase structure. Coatings with a dominant (411) plane orientation are known to exhibit enhanced corrosion resistance [9].

Conversely, on the copper substrate, NH_4Cl favors the γ-phase with the (101) orientation, as depicted in Figure 5.

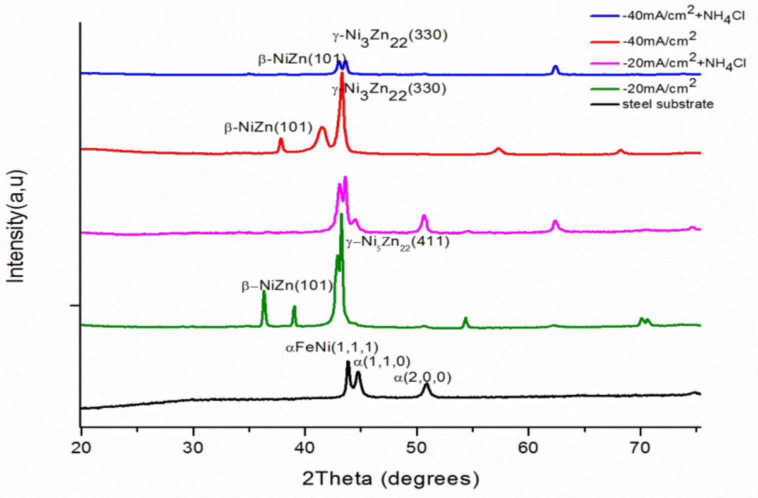

Figure 4. XRD patterns of the Ni–Zn deposits obtained on stainless steel substrate

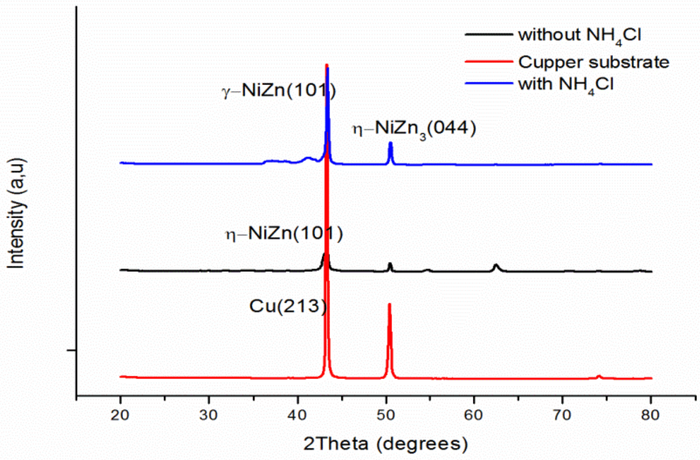

Figure 5. XRD patterns of the Ni–Zn deposits obtained on copper substrate

3.3. Corrosion behavior of deposits

3.3. 1. Potentiodynamic polarization studies

The corrosion behavior of Zn-Ni alloy coatings, deposited through chronopotentiometry on two different substrates (stainless steel and copper), was examined in an acidic medium (HCl 0.1 M). In relation to the polarization curves of Zn-Ni deposits on stainless steel in HCl 0.1 M (as shown in the figure), obtained both with and without NH_4Cl, it's observed that the corrosion current density of Zn-Ni prepared under -20 mA/cm^2 with NH_4Cl leads to cathodic control. This shift is attributed to the formation of a weak barrier layer that enhances anodic dissolution rates. The less noble nature of the deposit shifts the corrosion potentials (E_{corr}) of Zn-Ni coatings to more negative potentials, resulting in decreased corrosion potentials due to the low Ni content in the coatings and the presence of the η phase. The corrosion parameters J_{corr} (corrosion current density) and E_{corr} were determined using Tafel extrapolation.

The addition of Ni-Zn coatings shifts the E_{corr} to more noble potentials without NH_4Cl at -20 mA/cm^2, whereas with NH_4Cl, the increased Ni content still leads to more noble potentials, albeit with micro-cracks due to hydrogen release reduction.

Electrochemical parameters extracted from the polarization curves confirm that coatings obtained without NH_4Cl under -20 mA/cm^2 and -40 mA/cm^2 are more noble than samples obtained by chronopotentiometry with NH_4Cl. This difference can be attributed to the percentage of nickel in the deposit. However, the deposit obtained under -40 mA/cm^2 with NH_4Cl shows good content but with the presence of pores or micro-cracks in the Zn-Ni alloy layers, leading to increased hydrogen release and degradation of the deposit.

The shape of the curves strongly depends on the current density and NH_4Cl. This behavior can be attributed to the presence of the γ-Zn5Ni_{21} phase, which enhances the activation energy barrier of corrosion. Moreover, the substrate is visibly covered with brown corrosion products, indicating the good condition of the Zn-Ni samples.

The electrochemical results are in agreement with the literature, which suggests that coatings with Ni content between 12-16 wt% and a pure γ-Ni5Zn21 structure [10] exhibit the highest corrosion resistance. The shift of potential towards less noble values indicates an increase in sacrificial properties of Zn-Ni coatings, resulting from the dissolution of Zn from the coating, leading to increased Ni content [11].

The mechanism suggests that Zn-Ni corrosion produces a complex barrier layer consisting of a nickel-rich metallic phase and zinc corrosion products [12]. Initially, Zn-Ni could act as a sacrificial layer, undergoing anodic dissolution. Thermodynamically, zinc is preferentially oxidized, forming zinc-rich corrosion products and cracks in the metal coating. The remaining coating becomes enriched in nickel, resulting in higher nobility and the potential for local galvanic cells between Zn and Ni.

Interestingly, when depositing onto a copper substrate, the current efficiency changes compared to a stainless-steel substrate. The current density-potential curves for Zn-Ni alloys obtained on copper indicate different corrosive kinetics depending on the deposition current. The copper polarization curve shows cathodic control, leading to higher corrosion rates compared to a stainless-steel substrate.

In conclusion, the electrochemical behavior of Zn-Ni coatings follows expected trends and is consistent with prior research, showcasing the influence of Ni content, current density, and NH_4Cl on corrosion resistance and deposit morphology [13,14].

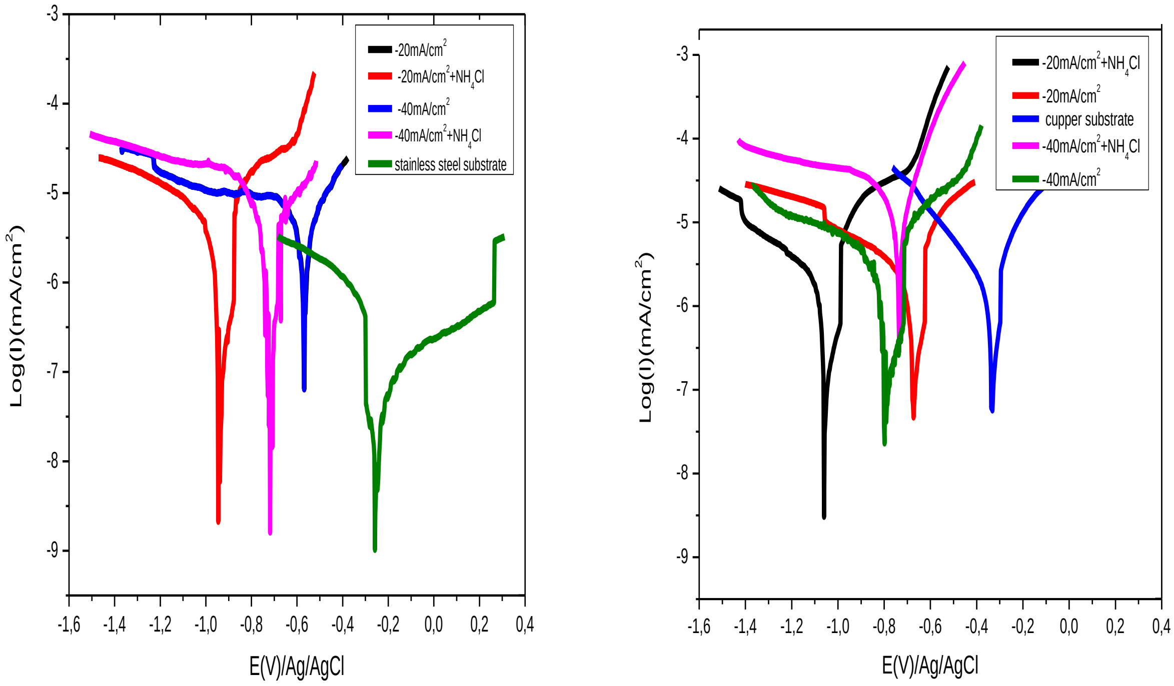

Figure 6. Potentiodynamic polarization curves of the Ni–Zn deposits obtained. (a) onto stainless steel; (b) onto cupper

3.3. 2. Electrochemical impedance spectroscopy (eis)

To gain deeper insights into the impact of Ni content on the corrosion resistance of Zn-Ni alloy in a 0.1 M HCl solution, impedance measurements were conducted and compared with the results obtained from Tafel plots. The impedance behavior of the investigated Zn-Ni alloys was analyzed in a 0.1 M HCl solution.

Figure 8 illustrates the Nyquist plots of two representative Zn-Ni alloys, I and IV, selected from the range of potentials between -100 mV and 100 mV relative to the open circuit potential (OCP). These plots were generated to confirm that the anodic process of the studied electrodes surpasses the cathodic process.

In other words, the impedance measurements were designed to assess the electrochemical behavior of the Zn-Ni alloys in the given acidic environment. The Nyquist plots provide valuable information about the complex impedance response of the alloys, shedding light on their corrosion resistance characteristics and the nature of the anodic and cathodic processes taking place.

These impedance measurements, when combined with the data from Tafel plots, enable a comprehensive understanding of how Ni content influences the corrosion resistance of Zn-Ni alloys in the specific HCl solution. By comparing the results from different electrochemical techniques, a more thorough picture of the corrosion behavior and mechanisms of the Zn-Ni alloys can be established.

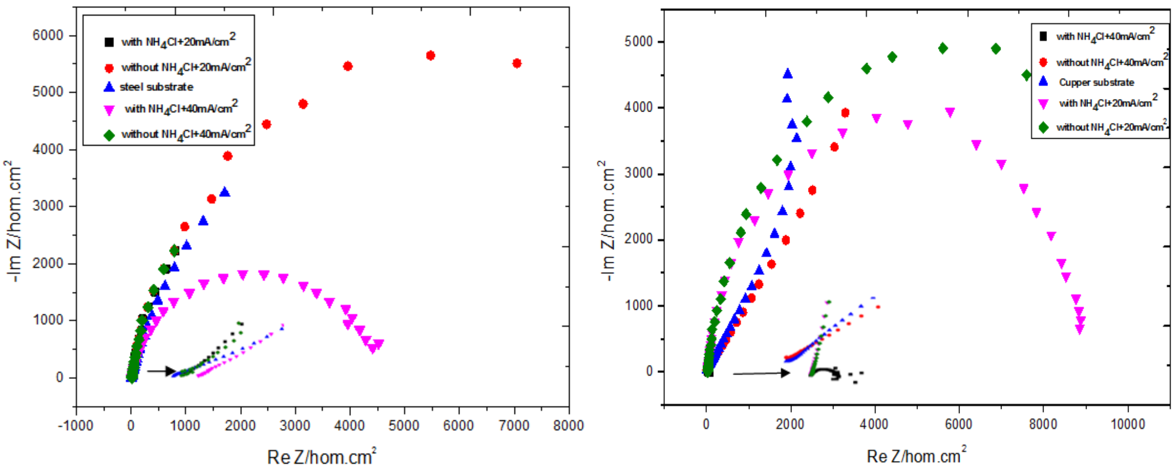

Figure 7. Nyquist responses of Zn–Ni alloy deposited on; (a) Stainless steel; (b) Copper

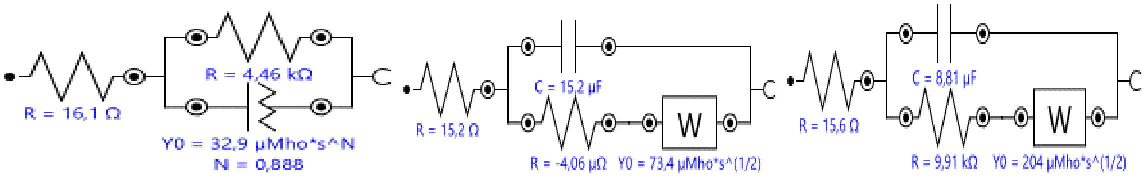

(a) **(b)** **(c)**

Figure 8. Equivalent circuit model used to fit impedance data on stainless steel AISI 304 ; (a) -20 mA/cm^2; (b)- -40 mA/cm^2;(c) -20 mA/cm^2+NH_4Cl

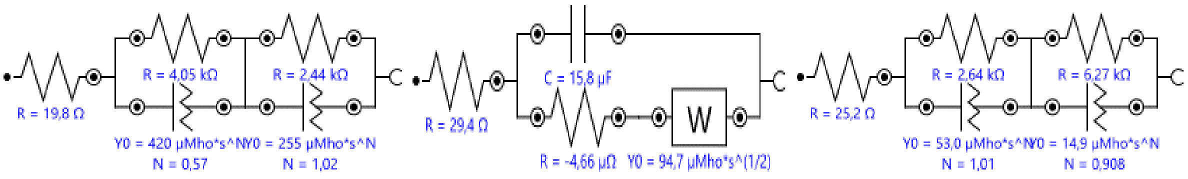

(a) **(b)** **(c)**

Figure 9. Equivalent circuit model used to fit impedance data on copper (a) -40 mA/cm^2 +NH_4Cl; (b) -40 mA/cm^2;(c) -20 mA/cm^2+NH_4Cl

Electrochemical impedance diagrams in Nyquist representation were constructed for the Zn-Ni deposits under both conditions of NH_4Cl presence and absence, at the two studied current densities, on a stainless-steel substrate. The recorded impedance spectra exhibit a single capacitive loop at the high-frequency range (HF), followed by a Warburg tail at low-frequency values (LF), as illustrated in the presence of NH4Cl at -20 mA/cm^2 (as shown in Figure 7). The observed Warburg impedance can be attributed to the diffusion of Zn species from the electrode surface into the bulk solution. To determine polarization resistance values, the Nyquist response was fitted to a simple equivalent circuit including components such as Re (electrolyte resistance), Rf and Cf (resistance and capacitance of the film), Rt (charge-transfer resistance), Cdc (double layer capacitance), CF (Faradic capacitance), RF (Faradic resistance), and Warburg element.

The polarization resistance ($R_p = R_e + R_f + R_t + R_F$) is plotted over time in Figure 7, along with |Ic| values for all coated surfaces produced via the galvanostatic technique. Meanwhile, the coating capacitance decreases as the cathodic current density decreases, indicating reduced corrosion intensity. Remarkably, the coating prepared under -20 mA/cm^2 in the presence of NH_4Cl exhibits the smallest capacitance value, notably 1.2142×10^{-5} μF/cm^2. This can be attributed to the excellent barrier properties of nickel within coatings after a partial chemical dissolution of zinc.

R_{tc} values demonstrate noticeable changes, especially in Zn-Ni deposits obtained under -40 mA/cm^2 without NH_4Cl, where the value increases to 31685 Ω.cm^2, indicating the stability of the protective systems. This performance suggests the presence of a passive layer on Zn-Ni alloys, contributing to their protective nature.

On the other hand, the Rt value increases for Zn-Ni deposits obtained without NH_4Cl on a copper substrate, suggesting progression towards a new stage of coating debonding. This increase can be related to the expansion of the debonding area due to media transformation in the tangential direction, leading to higher resistance to dielectric charge transfer. This results in a superposition effect, evident from the appearance of the W value, which confirms this phenomenon [15].

Furthermore, the Rt value significantly increases for Zn-Ni deposits on copper, particularly by approximately 2 times at -40 mA/cm^2 without NH_4Cl. This augmentation suggests a substantial charge transfer inhibition due to the presence of the γ-phase in electrodeposited Zn-Ni alloys. This change can also be affirmed by the alteration in the W value, representing a diffusion barrier affecting mass transfer processes.

4. CONCLUSION

In this study, Zn-Ni coatings were electrochemically deposited using an acidic bath with a pH of 4.86, incorporating NH_4Cl as an additive. Two main findings can be highlighted:

- The concentration of nickel within the coatings was influenced by factors such as cathodic current densities, the presence of NH_4Cl, and the type of substrate.
- The structure and morphology of the coatings exhibited variations based on the applied current density. Lower current densities resulted in the deposition of Zn-Ni coatings primarily composed of a single γ-Ni5Zn21 phase structure, containing Ni content in the range of 12-14%.

To assess the sacrificial behavior of the electrodeposited Zn-Ni coatings, polarization curves were employed. Additionally, electrochemical impedance spectroscopy (EIS) was utilized to evaluate the barrier properties of the coatings and their corrosion performance in a 0.1 M HCl solution.

The experimental results indicate that Zn-Ni alloy coatings obtained in the presence of NH_4Cl exhibit favorable electrochemical properties, demonstrating a protective effect on steel substrates. However, the sacrificial effect is more pronounced when these coatings are applied on copper substrates.

Moreover, the impact of applied current density becomes evident, as the deposits developed at -20 mA/cm^2 without NH_4Cl exhibit superior behavior compared to those obtained under different conditions.

In conclusion, this study sheds light on the intricate interplay between factors like current density, additive presence, and substrate type in shaping the properties and performance of Zn-Ni alloy coatings.

Declarations of interest

The authors declare no conflict of interest in this reported work.

REFERENCES

[1] M. Bielawski, Can. Aeronaut. Space J. 56 (2010) 67.

[2] S.P. Aggerholm, K. Søren, and D. Kim, J. Coat. Technol. Res. 6 (2009) 135.

[3] M. Kwon, D.H. Jo, S.H. Cho, H.T. Kim, J.T. Park, and J.M. Park, Surf. Coat. Technol. 288 (2016) 163.

[4] A. Conde, M.A. Arenas, and J.J. Damborenea, Corros. Sci. 53 (2011) 1489.

[5] M.G. Hosseini, H. Ashassi-Sorkhabi, and H.A.Y. Ghiasvand, Surf. Coat. Technol. 202 (2008) 2897.

[6] S. Cherevko, X. Xing, and C.H. Chung, Electrochem. Commun. 12 (2010) 467.

[7] A.C. Hegde, K. Venkatakrishna, and N. Eliaz, Surf. Coat. Technol 25 (2010) 2054.

[8] M.M. Abou-Krisha, Mater. Chem. Phys. 125 (2011) 621

[9] Y. Boonyongmaneerat, S. Saenapitak, and K. Saengkiettiyut, Alloys Compd. 487 (2009) 479.

[10] M.H. Sohi, and M. Jalali, J. Mater. Process. Technol. 138 (2003) 63.

[11] S.H. Mosavat, M.H. Shariat, and M.E. Bahrololoom, Corros. Sci. 59 (2012) 81.

[12] O. Hammami, L. Dhouibi, and E. Triki, Surf. Coat. Technol. 203 (2009) 2863.

[13] P. Fricoteaux, and C. Rousse, J. Electroanal. Chem. 612 (2008) 9.

[14] A. R. El-Sayed, H. S. Mohran, and H. M. Abd El-Lateef, J. Power. Sources 195 (2010) 6924.

[15] A. R. El-Sayed, H. S. Mohran, and H.M. Abd El-Lateef, J. Chin. Soc. Corr. Pro. 195 (2017) 479.